Science of the Total Environment 889 (2023) 164301

Contents lists available at ScienceDirect

Science of the Total Environment

journal homepage: www.elsevier.com/locate/scitotenv

Spatial variability of aerosol iron mineralogy and oxidation states over the Arctic Ocean

Songyun Fan [a], Barry Lai [b], Evert J. Elzinga [a], Ellery D. Ingall [c], Peter L. Morton [d,e], Yuan Gao [a,*]

[a] Department of Earth and Environmental Sciences, Rutgers University, Newark, NJ 07102, USA
[b] Advanced Photon Source, Argonne National Laboratory, Argonne, IL 60439, USA
[c] School of Earth and Atmospheric Sciences, Georgia Institute of Technology, Atlanta, GA 30332, USA
[d] Department of Oceanography, Texas A&M University, College Station, TX 77843, USA
[e] Geochemistry, National High Magnetic Field Laboratory, Tallahassee, FL 32310, USA

HIGHLIGHTS

- Western Arctic Ocean mineral aerosols are rich in hematite, ferrihydrite, while Alaska's aerosols predominantly contain biotite.
- Aerosol Fe oxidation state is more oxidized with increasing latitude.
- A significant correlation was found between Fe oxidation state and Fe fractional solubility.

GRAPHICAL ABSTRACT

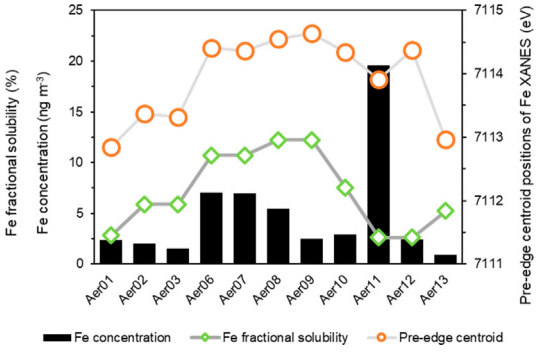

ARTICLE INFO

Editor: Hai Guo

Keywords:
Aerosol Fe mineralogy
Fe oxidation states
Arctic Ocean
XANES

ABSTRACT

The mineralogy and oxidation state of aerosol iron (Fe) play important roles in controlling aerosol Fe solubility and consequent bioavailability in seawater. In this study, the spatial variability of Fe mineralogy and oxidation states in aerosols collected during the US GEOTRACES Western Arctic cruise (GN01) were determined using synchrotron-based X-ray absorption near edge structure (XANES) spectroscopy. Both Fe(II) minerals (biotite, ilmenite) and Fe (III) minerals (ferrihydrite, hematite, Fe(III) phosphate) were found in these samples. However, aerosol Fe mineralogy and solubility observed during this cruise varied spatially and can be grouped into three clusters based on the air masses that affected aerosols collected in different regions: (1) biotite-enriched particles (87 % biotite, 13 % hematite) with the air masses passing over Alaska, showing relatively low Fe solubility (4.0 ± 1.7 %); (2) ferrihydrite-enriched particles (82 % ferrihydrite, 18 % ilmenite) collected in the remote Arctic air, showing relatively high Fe solubility (9.6 ± 3.3 %); (3) the fresh dust derived from North America and Siberia, primarily dominated by hematite (41 % hematite, 25 % Fe(III) phosphate, 20 % biotite, 13 % ferrihydrite), showing relatively low Fe solubility (5.1 ± 3.5). A significant positive correlation was found between Fe oxidation state and Fe fractional solubility, suggesting that long-range transport could modify iron (hydr) oxide such as ferrihydrite through atmospheric processing, influencing aerosol Fe solubility and consequently Fe bioavailability in the remote Arctic Ocean.

1. Introduction

The Arctic is experiencing rapid warming approximately twice as fast as the global average, known as Arctic amplification (Cohen et al., 2014;

* Corresponding author.
E-mail address: yuangaoh@newark.rutgers.edu (Y. Gao).

http://dx.doi.org/10.1016/j.scitotenv.2023.164301
Received 27 February 2023; Received in revised form 6 May 2023; Accepted 16 May 2023
Available online 20 May 2023

Serreze and Barry, 2011). Higher temperature has not only caused a significant reduction of sea ice coverage (Meier et al., 2007) but also increased terrestrial snow/ice-free areas during the summer (Ghatak et al., 2010). Exposure of active dust sources associated with glacial processes in Arctic regions is likely to enhance the dust emissions in some areas of the region (Bullard et al., 2016). Previous satellite observations showed that the dust plumes originating from southern Alaska and southern Iceland potentially contribute a substantial amount of nutrient trace elements to the surface seawater in the Gulf of Alaska (Crusius et al., 2011) and the North Atlantic (Prospero et al., 2012), respectively. In combination with the atmospheric processes (e.g., photoreduction, acidic reactions), atmospheric deposition was suggested to supply a nonnegligible amount of bioavailable iron (Fe) to the remote Canadian Arctic (De Vera et al., 2021).

Iron is a limiting micronutrient in marine biogeochemical cycles, which controls the primary production in up to one-third of the world ocean (Boyd and Ellwood, 2010; Falkowski, 1997; Martin and Fitzwater, 1988; Tagliabue et al., 2017). The bioavailability of Fe in dust aerosols is critical for evaluating the impacts of dust deposition on marine ecosystems (Ito and Shi, 2016; Mahowald et al., 2005), but the factors affecting the Fe bioavailability remain unclear. A common indicator of Fe bioavailability is fractional solubility, which describes the percentage of dissolved Fe that is readily used by microorganisms (Sholkovitz et al., 2012), although the experimental procedures for determining Fe solubility differ among various studies (Baker and Croot, 2010; Bowie et al., 2009; Buck et al., 2019; Clough et al., 2019; Edwards et al., 2006; Gao et al., 2013; Kumar et al., 2010; Mendez et al., 2010; Shelley et al., 2018; Siefert et al., 1999). Aerosol Fe mineralogy and Fe oxidation state were closely associated with Fe solubility and bioavailability (Ito et al., 2019; Journet et al., 2008; Schroth et al., 2009; Spolaor et al., 2013). Fe(II) minerals are usually considered to be more soluble and bioavailable than Fe(III), thus Fe in glacial flour enriched with Fe(II) minerals may be ~10 times more soluble than the Fe in Fe(III)-enriched tropical dust (Schroth et al., 2009). In addition, atmospheric processes, including photoreduction (Zhu et al., 1993; Zhuang et al., 1992), acidic reaction (Li et al., 2017; Ingall et al., 2018; Longo et al., 2016; Meskhidze et al., 2005; Nenes et al., 2011; Oakes et al., 2012; Shi et al., 2015; Baker et al., 2021), and organic complex association (Wiederhold et al., 2006; Xu and Gao, 2008) may significantly modify the Fe mineralogy and further control the Fe solubility in aerosols during long-range transport. Consequently, determining the Fe mineralogy and oxidation states in aerosols is necessary for a better understanding of aerosol Fe bioavailability as well as the effects of atmospheric processes during the long-range transport.

2. Methods

2.1. Sample collection and wet chemistry analysis

To characterize aerosol Fe mineralogy and oxidation states over the Arctic Ocean, aerosol sampling was carried out on the US GEOTRACES western Arctic cruise (GN01, also known as HLY1502) from Dutch Harbor, Alaska, to the North Pole between 9th August and 12th October 2015 on the US Coast Guard Cutter (USCGC) Healy (Fig. 1). Using a high-volume total suspended particulate (TSP) sampler (TE-5170V-BL, Tisch Environmental, USA), 14 bulk aerosol samples were collected during this cruise. In addition, 8 size-segregated particle samples were collected using a 10-stage Micro-Orifice Uniform Deposit Impactor (MOUDI, MSP Corp., MN, USA). Aerosol samplers were installed on the forward rail of Healy's flying bridge, ~23 m above sea level, to minimize the influence of sea spray. To minimize potential contamination from the stack exhaust, samplers were forward of the ship's stack and sampling was controlled by wind speed and direction, through a Campbell Scientific CR800 data-logger interfaced with an anemometer and wind vane set up near the samplers. Aerosol sampling was restricted to periods when in-sector conditions (defined as a relative wind direction from within $\pm 60^{\circ}$ of the ship's bow and a relative wind speed of >0.5 m s^{-1}) persisted for at least five continuous minutes. Sampling summary is given in Table 1. Bulk aerosol samples were used to characterize the major Fe mineralogy and Fe oxidation state. The total Fe concentrations in aerosol samples were determined through the application of strong-acid digestion of samples, followed by the analyses of the sample solutions using inductively coupled plasma-mass spectrometry. The soluble Fe concentrations were measured using UV/Vis spectroscopy with a modified Ferrozine method. Then, the fractional Fe solubility for each sample was estimated by the ratio of the soluble Fe concentration to the total Fe concentration. Detailed analytical methods can be found in Gao et al. (2019) for size-segregated aerosols and Marsay et al. (2018) for bulk aerosols.

2.2. Synchrotron-based X-ray analysis

To identify the major Fe mineralogy and oxidation states of the Fe-containing particles collected during the GN01 cruse in the Arctic Ocean, the X-ray absorption near edge structure (XANES) spectroscopy was performed at the beamline 2-ID-D Station of the Advanced Photon Source, DOE Argonne National Laboratory in Lemont, Illinois. Fourteen bulk aerosol samples were analyzed by Fe XANES to determine Fe mineralogy and Fe oxidation states. The pre-edge centroid of Fe XANES is a reliable indicator of Fe oxidation state (Wilke et al., 2001), and in this study it is used to reflect the variation of aerosol Fe oxidation states over the Arctic Ocean. More detailed methodology was discussed in Fan et al. (2022).

2.3. Data analysis

For data analyses, the Athena software's built-in function was used for the background correction and normalization of the original spectra (Ravel and Newville, 2005). We used the XANES dactyloscope software to subtract the baseline in order to isolate the pre-edge signals (Klementiev, 2002). Then pre-edge centroids were fitted by up to 4 Gaussian peaks using PeakFit 4.0 to estimate the pre-edge centroid positions. For assessing the major Fe composition, k-means clustering was used to group the sample Fe XANES. Principal component analysis (PCA) was performed to extract the main Fe composition in each group. Next, we conducted linear combination (LC) through the use of Athena software to obtain the major Fe composition. The following standards were used for LC fitting, which included Fe(II) oxide (FeO, >99.6 %, Sigma-Aldrich), Fe(II) oxalate ($FeC_2O_4{\cdot}2H_2O$, >99 %, Thermo Fisher), Fe(II) sulfate ($FeSO_4{\cdot}xH_2O$, >99.999 %, Sigma-Aldrich), Fe(III) oxalate ($Fe_2(C_2O_4)_3{\cdot}6H_2O$, >97 %, Thermo Fisher), Fe(III) sulfate ($Fe_2(SO_4)_3{\cdot}xH_2O$, >97 %, Sigma-Aldrich), Fe(III) phosphate ($FePO_4{\cdot}2H_2O$, Sigma-Aldrich), goethite (α-FeOOH, Sigma-Aldrich), and hematite (α-Fe_2O_3, 99.9 %, Atlantic Equipment Engineers). These are common standard materials that have been used for characterizing the composition of Fe-containing particles in other remote regions, such as the Antarctic Peninsula (Fan et al., 2022). To better quantify different Fe-containing particles, the spectra of biotite ($K(Mg,Fe)_3(AlSi_3O_{10})(F,OH)_2$), ferrihydrite ($Fe_2O_3{\cdot}0.5H_2O$), pyrite ($FeS_2$), and ilmenite ($FeTiO_3$) measured at the same beamline that were reported in Ingall et al. (2013) were also included in the LC fitting analysis of the data derived from this study. However, standards with low contributions to the LC fitting (<10 %) were eliminated, and this treatment included those which resulted in a poor fit. The pre-edge centroid positions were fitted by up to 5 Gaussian peaks and used to represent the variation of Fe oxidation states during data processing.

3. Results

3.1. Aerosol Fe minerology

Linear combination (LC) fitting of Fe K-edge XANES was used to determine aerosol Fe mineralogy over the Arctic Ocean (Fig. 3). Due to the low Fe loadings on sample filters of Aer4, Aer5, and Aer14, the Fe XANES of these three samples are not available, and therefore these samples were not included in this study. The major Fe-containing minerals include both Fe(II) minerals: biotite, ilmenite; and Fe (III) minerals: hematite, ferrihydrite. The k-means clustering identified two sample groups. The first

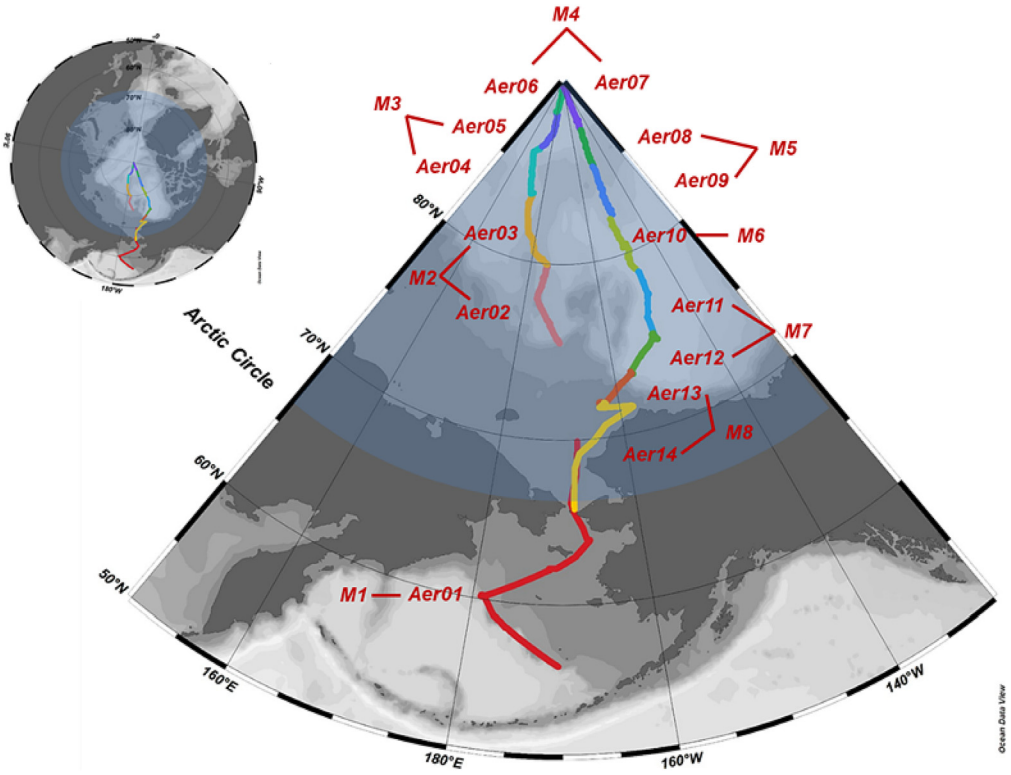

Fig. 1. Cruise track showing the locations of aerosol sampling along the cruise of the US GEOTRACES GN01. AerX and MX represent bulk samples and size-segregated samples, respectively.

group consists of the samples collected near the continental edge (Aer01 and Aer13). Biotite, a Fe(II) silicate, accounted for a high fraction of the total Fe in this group (Aer01: 87 % and Aer13: 39 %). Additionally, hematite (Aer01: 13 % and Aer13: 43 %) and ilmenite (Aer13: 18 %) were also found in these samples.

Samples in the second group were all collected over the remote Arctic Ocean. Variability in Fe-XANES spectra in this group suggests samples in this group received inputs from distinct sources during this cruise. Therefore, subclusters were generated by one more step k-means clustering. Samples Aer02–09 and Aer10–12 were grouped into two subclusters, respectively. To obtain the dominant Fe mineralogy, PCA was performed to extract the main features of Fe XANES for samples in the two clusters. The results of PCA indicated that the first main components could explain >99.8 % variance for both Aer02–09 and Aer10–12 groups. Consequently, the remaining components represent a very small fraction of the total Fe mass, and the first main components of the two subclusters were used to perform LCF to further determine the major Fe mineralogy in the remote Arctic Ocean. Samples Aer02–09 contained a high fraction of ferrihydrite

Table 1
Sampling information of aerosol bulk samples and size-segregated samples during the GN01 cruise.

Sample	Start date & time	Latitude (°N)	Longitude (°W)	End date & time	Latitude (°N)	Longitude (°W)	Air volume per filter (m^3)
Aer01	10 Aug 2015 17:53	56.07	170.51	17 Aug 2015 17:15	69.93	167.69	559.7 ± 115.4[a]
Aer02	20 Aug 2015 05:34	75.57	170.75	23 Aug 2015 18:12	80	174.95	173.7
Aer03	23 Aug 2015 19:21	80	174.96	27 Aug 2015 16:19	83.57	−174.73	270.4
Aer04	27 Aug 2015 20:49	83.76	−175.04	30 Aug 2015 21:40	86.24	−170.65	116
Aer05	30 Aug 2015 23:57	86.36	−171.69	04 Sep 2015 02:42	88.4	−176.64	12.8
Aer06	04 Sep 2015 10:02	88.41	−176.75	08 Sep 2015 04:34	89.94	97.85	275.6
Aer07	08 Sep 2015 06:05	89.94	104.19	12 Sep 2015 03:45	87.35	149.43	118.4
Aer08	12 Sep 2015 06:13	87.27	149.04	16 Sep 2015 04:30	85.15	149.85	72.7
Aer09	17 Sep 2015 00:20	85.16	150.40	20 Sep 2015 22:13	82.26	149.38	102.9
Aer10	21 Sep 2015 01:10	82.1	150.81	26 Sep 2015 03:05	78.97	148.5	321.3
Aer11	26 Sep 2015 04:38	78.80	148.09	29 Sep 2015 19:34	75.05	150.18	116.6
Aer12	29 Sep 2015 20:31	75.06	150.21	03 Oct 2015 16:25	73.43	156.79	211.8
Aer13	03 Oct 2015 18:41	73.4	156.77	07 Oct 2015 17:33	72	162.56	152.2
Aer14	07 Oct 2015 18:40	72	162.56	09 Oct 2015 23:50	65.95	168.45	90.5
M1	10 Aug 2015 17:53	56.07	170.51	17 Aug 2015 17:15	69.93	167.69	208.8
M2	20 Aug 2015 05:34	75.57	170.75	23 Aug 2015 18:19	83.57	−174.73	133.9
M3	27 Aug 2015 20:49	83.76	−175.04	04 Sep 2015 02:42	88.4	−176.64	54.8
M4	04 Sep 2015 10:02	88.41	−176.75	12 Sep 2015 03:45	87.35	149.43	119.2
M5	12 Sep 2015 06:13	87.27	149.04	20 Sep 2015 22:13	82.26	149.38	53.5
M6	21 Sep 2015 01:10	82.1	150.81	26 Sep 2015 03:05	78.97	148.5	99.0
M7	26 Sep 2015 20:31	78.80	148.09	03 Oct 2015 16:25	73.43	156.79	102.8
M8	03 Oct 2015 18:41	73.4	156.77	09 Oct 2015 23:50	65.95	168.45	74.3

[a] Sampling duration time for Aer01 sample is uncertain due to power problems.

(82 %) and a small fraction of ilmenite (18 %). In contrast, Fe in samples Aer10–12 were mainly in the form of hematite (41 %), with smaller fractions of Fe(III) phosphate (26 %), biotite (20 %), and ferrihydrite (13 %).

3.2. Variation of Fe oxidation state

Aerosol Fe oxidation state over the Arctic Ocean and Subarctic region varied noticeably during the cruise. Samples collected at lower latitudes had a high fraction of Fe(II), ~60–80 %, whereas this fraction dropped down to ~20 % in the high latitude samples. The variation of Fe oxidation state between individual samples is evident from the differences in the pre-edge centroid positions in the Fe XANES spectra (Fig. 4). The lowest two pre-edge centroid positions were found in the spectra of Aer01 (7112.8 eV) and Aer13 (7113.0 eV), which contained a high fraction of Fe(II) silicate, whereas the highest pre-edge centroid was found in sample Aer09 (7114.6 eV) which contained a high fraction of ferrihydrite. Sample Aer11 had an exceptionally high total Fe concentration (Fig. 4), which was attributed to high aeolian inputs from North America (Marsay et al., 2018). The Fe oxidation state of Aer11 (7113.9 eV) was significantly lower than that of Aer10 (7114.3 eV) and Aer12 (7114.4 eV), suggesting that the Fe oxidation state in dust originating from the crustal sources around the Arctic was relatively reduced compared to the aerosol Fe derived from other sources such as Chinese loess and African dust (Schroth et al., 2009). While the Fe fractional solubility varied during this cruise (Gao et al., 2019), a significant positive correlation ($p < 0.05$, $R^2 = 0.46$) between Fe fractional solubility and increasing Fe oxidation state was found (Fig. 4). This suggests that oxidation state could be an important factor affecting Fe solubility in aerosols during long-range transport.

4. Discussion

4.1. Sources of aerosol Fe

A previous study revealed that aerosol Fe collected during the GN01 cruise was primarily derived from crustal emissions (Marsay et al., 2018) and was dominated by coarse-mode aerosol particles (Gao et al., 2019). However, the Fe mineralogy showed notable changes in aerosols sampled in different regions during the cruise. As mentioned above, samples belonging to different clusters exhibited distinct Fe mineralogy. Interestingly, the clusters generated based on Fe XANES in this study agreed well with three sample clusters of aerosols impacted by different air mass types determined from air mass back-trajectories reported in Mukherjee et al. (2021) (Fig. 2), who worked with the same samples collected on this cruise. Mukherjee and colleagues divided the relevant air masses over the Arctic Ocean into three types: (1) air mass from the North Pacific and the Bering Sea regions; (2) entirely marine Arctic air; and (3) a mix of marine Arctic air with continental air mass, resulting in three corresponding sample clusters: (1) Aer01 (68 % type 1, 18 % type 2, and 15 % type 3); (2) Aer02–09 (100 % type 2); and (3) Aer10–13 (35 % type 2, 65 % type 3). The Fe in Aer01 impacted by the type 1 air mass originated from the North Pacific and the Bering Sea regions and contained a high fraction of the Fe(II)-silicate biotite. Aeolian dust derived from glacial sediment was suggested to be an important source of bioavailable Fe during the summer in Alaska, attributed to the exposed sediments due to the low river levels and reduced snow cover, and the dust plume over the Gulf of Alaska sometimes can even be observed by satellites (Crusius et al., 2011). The principal Fe-containing mineral in Alaska glacial flour was biotite, which accounted for 30–60 % of the total Fe (Schroth et al., 2009). Similarly, a high fraction of biotite was also found in mineral dust particles over the Antarctic Peninsula which were possibly originated from glacial flour as well (Fan et al., 2022). Aer01 and Aer13 were sampled close to Alaska (Fig. 1) and found to contain a high fraction of biotite, which agrees well with the results of Schroth et al. (2009).

When the cruise entered the remote Arctic Ocean, Fe(III) minerals predominated. The major Fe mineralogy of Aer02-Aer09 was dominated by ferrihydrite. Ferrihydrite is widely found in dust aerosols and aerosol source materials, including soils in arid regions and glacial flour (Schroth et al., 2009; Takahashi et al., 2011). Ferrihydrite was also found to be a major composition in aerosol Fe in the remote Pacific Ocean, affecting the Fe fractional solubility in marine aerosols far from the continent (Kurisu et al., 2021). In addition, the abundance of ferrihydrite increased with increasing traveling distance and time for acidic reactions (Sakata et al., 2022). The air mass back trajectories suggest that aerosol particles in remote Arctic air traveled a long distance and were relatively aged (Mukherjee et al., 2021). A previous study has suggested that atmospheric chemical processing of clay minerals may lead to the formation of ferrihydrite during long-range transport (Takahashi et al., 2011). Although the dust aerosols in the Arctic are primarily derived from the Asian and African deserts (Fan, 2013; Vincent, 2018), the calculated back trajectories

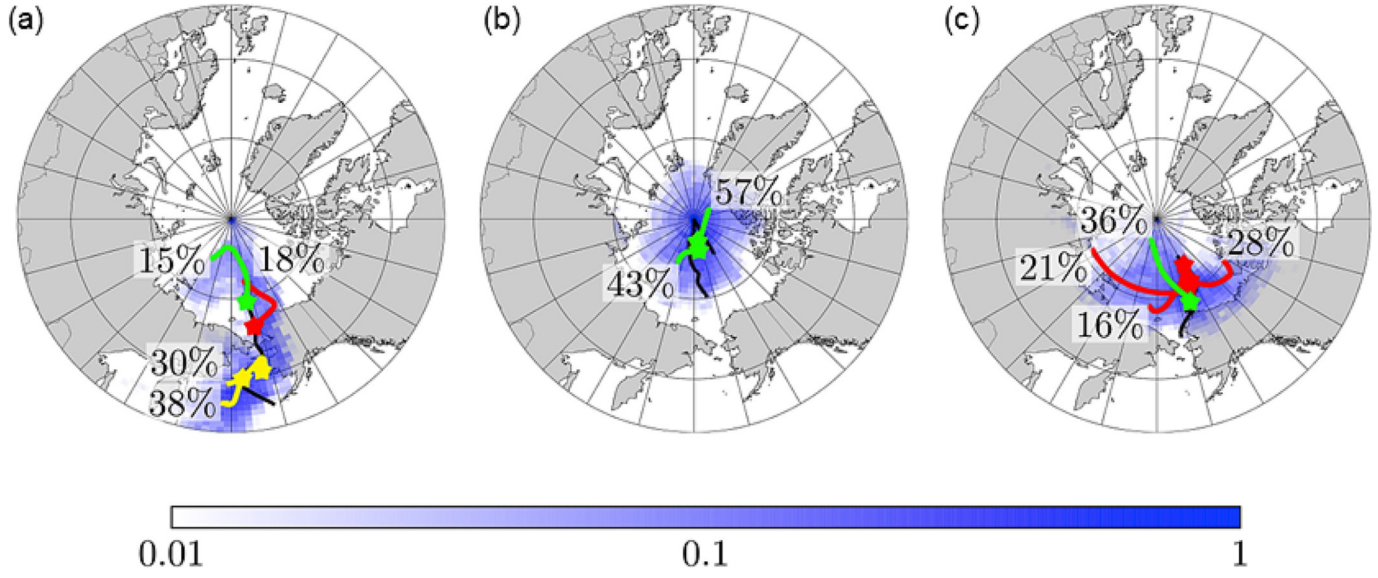

Fig. 2. Results of air mass back trajectory analysis with the NOAA HYSPLT4 model from Mukherjee et al. (2021) for (a) group 1 samples, (b) group 2 samples, and (c) group 3 samples. The lines with different colors represent the relative impact of distinct sources: type 1: yellow, type 2: green, and type 3: red. The cruise track is shown in black line. The relative spatial frequency of 100 h back-trajectories was calculated and represented by the shades of blue.

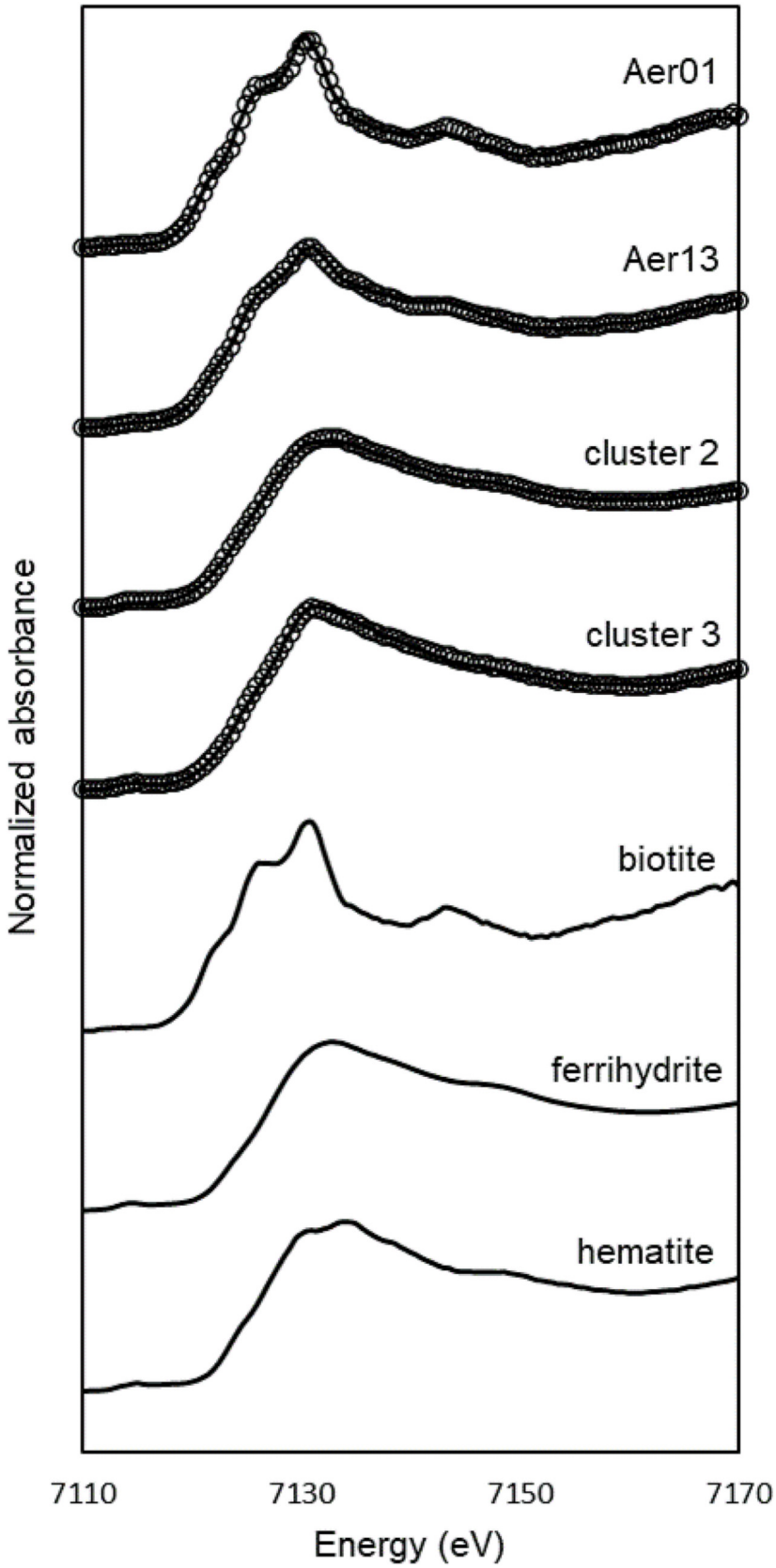

Fig. 3. The results of linear combination fitting in this study. Solid lines and cycles represent the measured spectra and fitting results, respectively.

for 100 h in this cluster did not pass over any continental region (Mukherjee et al., 2021), implying that the mineral dust traveled for at least 100 h providing ample time for atmospheric chemical reactions.

Air mass back trajectories suggested that Aer10-Aer12 received air from the remote Arctic and from continental northern Russia and Canada as well (Mukherjee et al., 2021). The major Fe-containing minerals in these

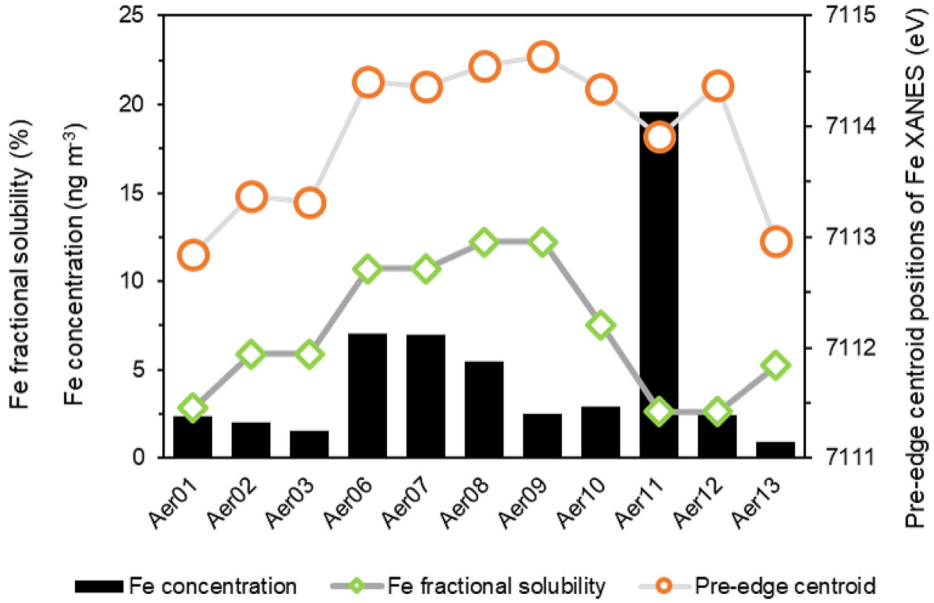

Fig. 4. The variations of pre-edge centroid positions of Fe K-edge XANES, Fe concentrations, and Fe fractional solubility in aerosols during the GN01 cruise (Gao et al., 2019; Marsay et al., 2018). Each pair of the bulk samples (Aer02/03, Aer06/Aer07, Aer08/Aer09, and Aer11/Aer12) corresponded to one size-segregated sample for Fe solubility, as two bulk samples were collected while only one size-segregated sample was collected in the same period of time.

samples are more diverse and include hematite, Fe(III)-phosphate, biotite, and ferrihydrite. As discussed above, biotite and ferrihydrite were likely derived from glacial flour from high latitude continents and affected by atmospheric chemical processes during long-range transport. Hematite is a common Fe mineral widely found in soils in tropical areas (Cornell and Schwertmann, 2003). However, Fe(III) phosphate is not typically found in natural environments at high concentrations, and may be a product of atmospheric acidic processes (Ingall et al., 2018). Therefore, in addition to the source material of aerosol Fe, atmospheric processing could play a critical role in modifying Fe mineralogy during long range transport over the Arctic. Although anthropogenic sources could contribute to aerosol Fe (Ito et al., 2019; Sedwick et al., 2007; Petroselli et al., 2019), the calculations of crustal enrichment factors for the samples collected during this cruise suggest that in general aerosol Fe was primarily derived from crustal sources (Gao et al., 2019; Marsay et al., 2018).

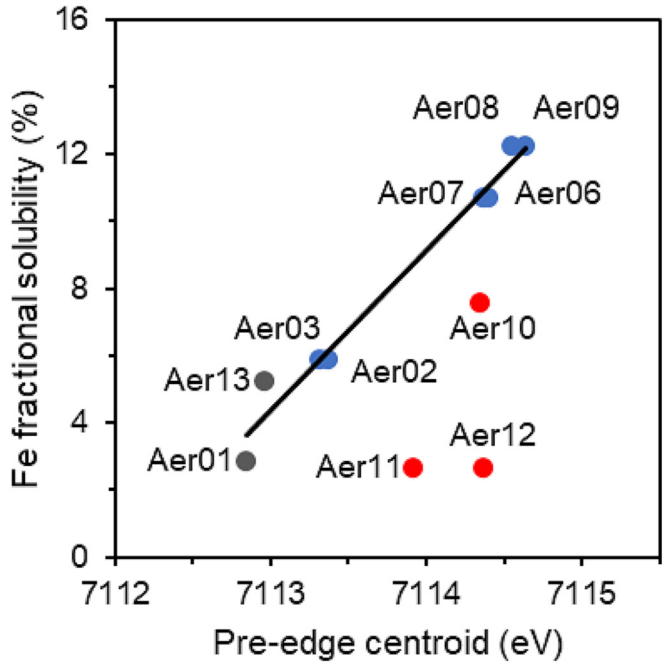

Fig. 5. The correlation between pre-edge centroid and aerosol Fe fractional solubility. Grey points are biotite-enriched particles (type 1), blue points are ferrihydrite-enriched particles (type 2), and red points are hematite-enriched particles (type 3). The red points were treated as outliers and not included for regression.

4.2. Aerosol Fe oxidation state and bioavailability

The oxidation state has a significant impact on the Fe solubility, with Fe (II) species generally showing higher bioavailability than Fe(III) (Spolaor et al., 2013). In the current study, aerosol Fe solubility was positively correlated with an increased Fe oxidation state (Fig. 5). This suggests that Fe oxidation state could contribute to the variation in Fe solubility.

Biotite and ilmenite are the major Fe(II) minerals found in aerosol samples analyzed from the GN01 cruise. Although the Fe silicates in biotite-enriched glacial flour were suggested to be more soluble than the Fe(III) minerals in tropical dust, the Fe fractional solubility in glacial flour is only ~0.1–1 % (Schroth et al., 2009). In contrast, the highest Fe fractional solubility was found in the samples collected in the remote Arctic Ocean including the North Pole during this cruise, and these particles were predominantly under the influence of the Arctic marine air based on the air-mass back trajectories and aged. Consequently, ferrihydrite produced by atmospheric processing likely dominated the major Fe mineralogy in these samples. A previous study indicated that chlorite in Asian dust can be transformed into ferrihydrite during long-range transport, and that this process significantly increased the Fe fractional solubility (Takahashi et al., 2011). Both biotite and chlorite are Fe-containing phyllosilicates, and their Fe XANES spectra closely resemble each other (O'Day et al., 2004). Therefore, given that Asian desserts are the primary source of dust aerosols over the Arctic Ocean (Vincent, 2018), the atmospheric processes might transform Fe silicate into ferrihydrite during long-range transport. It is worth noting that the solubility of ferrihydrite may change with time. For instance, dry ferrihydrite is much less soluble than fresh ferrihydrite (Raiswell et al., 2010). The Fe fractional solubility in our ferrihydrite-enriched samples was 9.6 ± 3.0 % (Gao et al., 2019), which is much higher than the ferrihydrite-enriched dust samples (<0.1 % total solubility after three leaches) reported in Schroth et al. (2009). This suggests that the ferrihydrite in our samples was not fresh source materials but was modified through atmospheric processes. The correlation between Fe fractional solubility and Fe oxidation states in type 1 and type 2 samples (Fig. 5) may

Table 2
Fe fractional solubility, dry deposition flux, pre-edge centroid, and Fe mineralogy in aerosols over the western Arctic Ocean.

	HV	MOUDI	SFe(II)[a] (%)	SFeD[a] (%)	Fe(II) deposition[a] ($\mu mol\ m^{-2}\ yr^{-1}$)	FeT deposition[a] ($\mu mol\ m^{-2}\ yr^{-1}$)	Pre-edge centroid of Fe XANES (eV)	Fe mineralogy
Group 1	Aer01, Aer13	M1, M8	2.3–4.3	2.9–5.2	0.031–0.034	4.2–6.5	7122.8–7113.0	Biotite, hematite
Group 2	Aer02-Aer09	M2-M5	3.3–8.6	5.9–12	0.054–0.13	0.76–5.6	7113.3–7114.6	Ferrihydrite, ilmenite
Group 3	Aer10-Aer12	M6-M7	2.5–5.3	2.6–7.6	0.025–0.13	2.6–6.0	7113.9–7114.4	Hematite, Fe(III) phosphate, biotite, ferrihydrite

[a] Data from Gao et al. (2019).

result from the oxidation of Fe(II) in minerals, such as biotite to ferrihydrite. The oxidation process is likely more extensive in samples with longer transport times and thus, could enhance both the fraction of ferrihydrite in the total Fe and Fe fractional solubility. Part of the cruise (Aer11) directly received air masses from continental sources, including North America and Siberia (Fig. 4) (Marsay et al., 2018). The Fe fractional solubility of these samples (type 3) was significantly lower than the type 2 samples (Fig. 4), which may be related to a decrease of the soluble ferrihydrite fraction and increases in the hematite and biotite fractions.

In addition to the processes of modifying Fe minerals during long-range transport, other processes affect Fe solubility as well. Atmospheric photoreduction (Zhu et al., 1993; Zhuang et al., 1992) and acidic reaction (Ingall et al., 2018; Longo et al., 2016; Nenes et al., 2011; Shi et al., 2015) can modify the Fe mineralogy and affect Fe solubility. In Gao et al. (2019), soluble Fe(II) accounted for 2.3 % to 8.6 %, of total Fe with a mean of 4.9 %. This was substantially lower than the percentage contribution of overall Fe(II) to the total Fe in the samples (18 %–87 %), indicating that a large portion of Fe(II) was not soluble. However, Fe(II) accounted for 55 %–96 % of the total soluble Fe. The extremely high Fe(II) fraction of the total soluble Fe is evidence that part of soluble Fe(III) might be reduced to Fe(II) through atmospheric processes such as photoreduction. Furthermore, Fe(III) phosphate was suggested to be a product of acidic reaction since it does not commonly exist in the natural environment at high concentrations (Ingall et al., 2018). Therefore, our results suggest that atmospheric processing, which may include cloud processing (Fan, 2013; Shi et al., 2015), organic ligand dissociation (Wiederhold et al., 2006), acidic reaction (Ingall et al., 2018), and photoreduction (Zhu et al., 1993), is an important factor affecting the aerosol Fe mineralogy over the Arctic Ocean.

In this study, the relatively high fractional solubility over the remote Arctic Ocean was possibly attributed to the modification of Fe mineralogy in aged dust particles, indicating that the solubility and consequent bioavailability of aerosol Fe could be enhanced during the atmospheric long-range transport. The Fe fractional solubility and Fe(II) fractional solubility in coastal sites (groups 1 and 3) were lower than the remote sites (Gao et al., 2019), as shown in Table 2. Although the deposition fluxes of total Fe in coastal regions were higher than the remote regions, both Fe fractional solubility and Fe(II) fractional solubility were lower in these regions, resulting in lower deposition fluxes of bioavailable Fe compared to those in the high Arctic. These results suggest that the atmospheric deposition potentially supply more soluble Fe in the remote Arctic Ocean affected by the processes during atmospheric long-range transport, which could potentially impact the marine ecosystems in the remote Arctic Ocean.

5. Conclusions

Fe mineralogy in aerosols in air masses from different source regions over the Arctic Ocean can be divided into three clusters: (1) High fraction of biotite with relatively low Fe oxidation states and low Fe solubility derived from Alaskan glacial flour; (2) ferrihydrite with high Fe oxidation states and the highest Fe solubility contributed by remote Arctic air; and (3) hematite with relatively high oxidation states and low Fe solubility derived from fresh continental dust (mostly North America and Siberia). A positive correlation between Fe oxidation state and Fe fractional solubility suggests that atmospheric processes could transform Fe-containing minerals, such as biotite, into ferrihydrite and increase Fe fractional solubility. Although the percentage of Fe(II) dropped to approximately 20 % in the remote Arctic Ocean, the soluble Fe(II) still accounted for 55 %–70 % in the total soluble Fe. Many atmospheric processes likely contribute to the observed Fe (II) during this study. Photochemical reduction under sunlight may produce Fe(II) in marine aerosols (Zhu et al., 1993). The processing in acidic cloud waters may also affect Fe dissolution in dust, leading to the production of Fe(II) (Desboeufs et al., 2003). Therefore, we conclude that the aerosol Fe bioavailability in the remote Arctic Ocean should be higher than the freshly emitted dust close to the continental margin. Further studies involving more detailed mineralogy methods such as extended X-ray absorption fine structure (EXAFS) with more samples for analyses are needed to precisely quantify the Fe mineralogy over the different regions in the Arctic.

CRediT authorship contribution statement

Songyun Fan: Lab experiments, Data analysis, Writing-Original draft and revisions. **Barry Lai**: Lab experiments, Writing-Reviewing and Editing, Data analysis. **Evert J. Elzinga and Ellery D. Ingall**: Writing-Reviewing and Editing. **Peter** L. **Morton**: Sample Preparation, Reviewing and Editing. **Yuan Gao**: Conceptualization, Project administration, Lab experiments, Writing-Reviewing and Editing, Funding acquisition.

Data availability

Data will be made available on request.

Declaration of competing interest

The authors declare that they have no known competing financial interests or personal relationships that could have appeared to influence the work reported in this paper.

Acknowledgements

This research was sponsored by the US National Science Foundation Grants OCE-2048858 (YG), OCE-1435871 (YG), OCE-1436019 (PLM) and OCE-1658311 (PLM). Sample analyses were performed on Beamline 2-ID-D at the Advanced Photon Source, a US Department of Energy Office of Science User Facility operated by Argonne National Laboratory, under Contract No. DE-AC02-06CH11357. The National High Magnetic Field Laboratory is supported by National Science Foundation Cooperative Agreements No. DMR-1157490/1644779 and the State of Florida. We are grateful to Christopher Marsay, Clifton Buck, William Landing for assistance with sampling, and Pami Mukherjee, Shun Yu, Rafael Jusino-Atresino, and Guojie Xu for assistance with air sampling preparation. We also thank Jianqiong Zhan for help with meteorological data analyses. This work would not have become possible without the dedication of the crew of the USCGC Healy at sea.

References

Baker, A.R., et al., 2021. Changing atmospheric acidity as a modulator of nutrient deposition and ocean biogeochemistry. Sci. Adv. 7, eabd8800. https://doi.org/10.1126/sciadv.abd8800.

Baker, A.R., Croot, P.L., 2010. Atmospheric and marine controls on aerosol iron solubility in seawater. Mar. Chem. 120 (1–4), 4–13.

Bowie, A.R., Lannuzel, D., Remenyi, T.A., Wagener, T., Lam, P.J., Boyd, P.W., ... Trull, T.W., 2009. Biogeochemical iron budgets of the Southern Ocean south of Australia: decoupling of iron and nutrient cycles in the subantarctic zone by the summertime supply. Glob. Biogeochem. Cycles 23 (4).

Boyd, P.W., Ellwood, M.J., 2010. The biogeochemical cycle of iron in the ocean. Nat. Geosci. 3 (10), 675–682. https://doi.org/10.1038/ngeo964.
Buck, C.S., Aguilar-Islas, A., Marsay, C., Kadko, D., Landing, W.M., 2019. Trace element concentrations, elemental ratios, and enrichment factors observed in aerosol samples collected during the US GEOTRACES eastern Pacific Ocean transect (GP16). Chem. Geol. 511, 212–224.
Bullard, J.E., et al., 2016. High-latitude dust in the Earth system. Rev. Geophys. 54 (2), 447–485. https://doi.org/10.1002/2016RG000518.
Clough, R., Lohan, M.C., Ussher, S.J., Nimmo, M., Worsfold, P.J., 2019. Uncertainty associated with the leaching of aerosol filters for the determination of metals in aerosol particulate matter using collision/reaction cell ICP-MS detection. Talanta 199, 425–430.
Cohen, J., et al., 2014. Recent Arctic amplification and extreme mid-latitude weather. Nat. Geosci. 7 (9), 627–637. https://doi.org/10.1038/ngeo2234.
Cornell, R.M., Schwertmann, U., 2003. The Iron Oxides: Structure, Properties, Reactions, Occurrences, and Uses. Wiley-vch Weinheim.
Crusius, J., Schroth, A.W., Gassó, S., Moy, C.M., Levy, R.C., Gatica, M., 2011. Glacial flour dust storms in the Gulf of Alaska: hydrologic and meteorological controls and their importance as a source of bioavailable iron. Geophys. Res. Lett. 38 (6). https://doi.org/10.1029/2010GL046573.
De Vera, J., Chandan, P., Landing, W.M., Stupple, G.W., Steffen, A., Bergquist, B.A., 2021. Amount, sources, and dissolution of aerosol trace elements in the Canadian Arctic. ACS Earth Space Chem. 5 (10), 2686–2699. https://doi.org/10.1021/acsearthspacechem.1c00132.
Desboeufs, K.V., Losno, R., Colin, J.L., 2003. Relationship between droplet pH and aerosol dissolution kinetics: effect of incorporated aerosol particles on droplet pH during cloud processing. J. Atmos. Chem. 46 (2), 159–172. https://doi.org/10.1023/A:1026011408748.
Edwards, R., Sedwick, P., Morgan, V., Boutron, C., 2006. Iron in ice cores from Law Dome: a record of atmospheric iron deposition for maritime East Antarctica during the Holocene and Last Glacial Maximum. Geochem. Geophys. Geosyst. 7 (12).
Falkowski, P.G., 1997. Evolution of the nitrogen cycle and its influence on the biological sequestration of CO2 in the ocean. Nature 387 (6630), 272–275. https://doi.org/10.1038/387272a0.
Fan, S., Gao, Y., Lai, B., Elzinga, E.J., Yu, S., 2022. Aerosol iron speciation and seasonal variation of iron oxidation state over the western Antarctic Peninsula. Sci. Total Environ. 824, 153890. https://doi.org/10.1016/j.scitotenv.2022.153890.
Fan, S.-M., 2013. Modeling of observed mineral dust aerosols in the arctic and the impact on winter season low-level clouds. J. Geophys. Res. Atmos. 118 (19), 11,161–111,174. https://doi.org/10.1002/jgrd.50842.
Gao, Y., Marsay, C.M., Yu, S., Fan, S., Mukherjee, P., Buck, C.S., Landing, W.M., 2019. Particle-size variability of aerosol iron and impact on iron solubility and dry deposition fluxes to the Arctic Ocean. Sci. Rep. 9 (1), 16653. https://doi.org/10.1038/s41598-019-52468-z.
Gao, Y., Xu, G., Zhan, J., Zhang, J., Li, W., Lin, Q., ... Lin, H., 2013. Spatial and particle size distributions of atmospheric dissolvable iron in aerosols and its input to the Southern Ocean and coastal East Antarctica. J. Geophys. Res. Atmos. 118 (22), 12–634.
Ghatak, D., Frei, A., Gong, G., Stroeve, J., Robinson, D., 2010. On the emergence of an Arctic amplification signal in terrestrial Arctic snow extent. J. Geophys. Res. Atmos. 115 (D24). https://doi.org/10.1029/2010JD014007.
Ingall, E.D., et al., 2013. Role of biogenic silica in the removal of iron from the Antarctic seas. Nat. Commun. 4 (1), 1981. https://doi.org/10.1038/ncomms2981.
Ingall, E.D., et al., 2018. Enhanced iron solubility at low pH in global aerosols. Atmosphere 9 (5), 201.
Ito, A., Shi, Z., 2016. Delivery of anthropogenic bioavailable iron from mineral dust and combustion aerosols to the ocean. Atmos. Chem. Phys. 16 (1), 85–99. https://doi.org/10.5194/acp-16-85-2016.
Ito, A., Myriokefalitakis, S., Kanakidou, M., Mahowald, N.M., Scanza, R.A., Hamilton, D.S., Baker, A.R., Jickells, T., Sarin, M., Bikkina, A.S., Gao, Y., Shelley, R.U., Buck, C.S., Landing, W.M., Bowie, A.R., Perron, M.M.G., Guieu, C., Meskhidze, N., Johnson, M.S., Feng, Y., Kok, J.F., Nenes, A., Duce, R.A., 2019. Pyrogenic iron: the missing link to high iron solubility in aerosols. Sci. Adv. 5 (5), eaau7671.
Journet, E., Desboeufs, K.V., Caquineau, S., Colin, J.-L., 2008. Mineralogy as a critical factor of dust iron solubility. Geophys. Res. Lett. 35 (7). https://doi.org/10.1029/2007GL031589.
Klementiev, K., 2002. XANES dactyloscope for Windows. KV Klementiev, XANES Dactyloscope for Windows *freeware: www.desy.de/~klmn/xanda.html.*
Kumar, A., Sarin, M.M., Srinivas, B., 2010. Aerosol iron solubility over Bay of Bengal: role of anthropogenic sources and chemical processing. Mar. Chem. 121 (1–4), 167–175.
Kurisu, M., Sakata, K., Uematsu, M., Ito, A., Takahashi, Y., 2021. Contribution of combustion Fe in marine aerosols over the northwestern Pacific estimated by Fe stable isotope ratios. Atmos. Chem. Phys. 21 (20), 16027–16050.
Li, Weijun, et al., 2017. Air pollution–aerosol interactions produce more bioavailable iron for ocean ecosystems. Sci. Adv. 3 (3), e1601749. https://doi.org/10.1126/sciadv.1601749.
Longo, A.F., Feng, Y., Lai, B., Landing, W.M., Shelley, R.U., Nenes, A., Mihalopoulos, N., Violaki, K., Ingall, E.D., 2016. Influence of atmospheric processes on the solubility and composition of Iron in Saharan Dust. Environ. Sci. Technol. 50 (13), 6912–6920. https://doi.org/10.1021/acs.est.6b02605.
Mahowald, N.M., Baker, A.R., Bergametti, G., Brooks, N., Duce, R.A., Jickells, T.D., Kubilay, N., Prospero, J.M., Tegen, I., 2005. Atmospheric global dust cycle and iron inputs to the ocean. Glob. Biogeochem. Cycles 19 (4). https://doi.org/10.1029/2004GB002402.
Marsay, C.M., Kadko, D., Landing, W.M., Morton, P.L., Summers, B.A., Buck, C.S., 2018. Concentrations, provenance and flux of aerosol trace elements during US GEOTRACES Western Arctic cruise GN01. Chem. Geol. 502, 1–14. https://doi.org/10.1016/j.chemgeo.2018.06.007.
Martin, J.H., Fitzwater, S.E., 1988. Iron deficiency limits phytoplankton growth in the north-east Pacific subarctic. Nature 331 (6154), 341–343. https://doi.org/10.1038/331341a0.
Meier, W.N., Stroeve, J., Fetterer, F., 2007. Whither Arctic sea ice? A clear signal of decline regionally, seasonally and extending beyond the satellite record. Ann. Glaciol. 46, 428–434. https://doi.org/10.3189/172756407782871170.
Mendez, J., Guieu, C., Adkins, J., 2010. Atmospheric input of manganese and iron to the ocean: seawater dissolution experiments with Saharan and North American dusts. Mar. Chem. 120 (1–4), 34–43.
Meskhidze, N., Chameides, W.L., Nenes, A., 2005. Dust and pollution: a recipe for enhanced ocean fertilization? J. Geophys. Res. Atmos. 110 (D3).
Mukherjee, P., Marsay, C.M., Yu, S., Buck, C.S., Landing, W.M., Gao, Y., 2021. Concentrations and size-distributions of water-soluble inorganic and organic species on aerosols over the Arctic Ocean observed during the US GEOTRACES Western Arctic Cruise GN01. Atmos. Environ. 261, 118569. https://doi.org/10.1016/j.atmosenv.2021.118569.
Nenes, A., Krom, M.D., Mihalopoulos, N., Van Cappellen, P., Shi, Z., Bougiatioti, A., Zarmpas, P., Herut, B., 2011. Atmospheric acidification of mineral aerosols: a source of bioavailable phosphorus for the oceans. Atmos. Chem. Phys. 11 (13), 6265–6272. https://doi.org/10.5194/acp-11-6265-2011.
Oakes, M., Ingall, E.D., Lai, B., Shafer, M.M., Hays, M.D., Liu, Z.G., Weber, R.J., 2012. Iron solubility related to particle sulfur content in source emission and ambient fine particles. Environ. Sci. Technol. 46 (12), 6637–6644.
O'Day, A.P., Nelson, R., Root, R., Carroll, S.A., 2004. X-ray absorption spectroscopic study of Fe reference compounds for the analysis of natural sediments. Am. Mineral. 89 (4), 572–585. https://doi.org/10.2138/am-2004-0412.
Petroselli, C., Moroni, B., Crocchianti, S., Selvaggi, R., Vivani, R., Soggia, F., Grotti, M., D'Acapito, F., Cappelletti, D., 2019. Iron speciation of natural and anthropogenic dust by spectroscopic and chemical methods. Atmosphere 10 (1), 8.
Prospero, J.M., Bullard, J.E., Hodgkins, R., 2012. High-latitude dust over the North Atlantic: inputs from Icelandic proglacial dust storms. Science 335 (6072), 1078–1082. https://doi.org/10.1126/science.1217447.
Raiswell, R., Vu, H.P., Brinza, L., Benning, L.G., 2010. The determination of labile Fe in ferrihydrite by ascorbic acid extraction: methodology, dissolution kinetics and loss of solubility with age and de-watering. Chem. Geol. 278 (1), 70–79. https://doi.org/10.1016/j.chemgeo.2010.09.002.
Ravel, B., Newville, M., 2005. ATHENA, ARTEMIS, HEPHAESTUS: data analysis for X-ray absorption spectroscopy using IFEFFIT. J. Synchrotron Radiat. 12 (4), 537–541.
Sakata, K., Kurisu, M., Takeichi, Y., Sakaguchi, A., Tanimoto, H., Tamenori, Y., Takahashi, Y., 2022. Iron (Fe) speciation in size-fractionated aerosol particles in the Pacific Ocean: the role of organic complexation of Fe with humic-like substances in controlling Fe solubility. Atmos. Chem. Phys. 22 (14), 9461–9482.
Schroth, A.W., Crusius, J., Sholkovitz, E.R., Bostick, B.C., 2009. Iron solubility driven by speciation in dust sources to the ocean. Nat. Geosci. 2 (5), 337–340. https://doi.org/10.1038/ngeo501.
Sedwick, P.E., Sholkovitz, E.R., Church, T.M., 2007. Impact of anthropogenic combustion emissions on the fractional solubility of aerosol iron: evidence from the Sargasso Sea. Geochem. Geophys. Geosyst. 8, Q10Q06.
Serreze, M.C., Barry, R.G., 2011. Processes and impacts of Arctic amplification: a research synthesis. Glob. Planet. Chang. 77 (1), 85–96. https://doi.org/10.1016/j.gloplacha.2011.03.004.
Shelley, R.U., Landing, W.M., Ussher, S.J., Planquette, H., Sarthou, G., 2018. Regional trends in the fractional solubility of Fe and other metals from North Atlantic aerosols (GEOTRACES cruises GA01 and GA03) following a two-stage leach. Biogeosciences 15 (8), 2271–2288.
Shi, Z., Krom, M.D., Bonneville, S., Benning, L.G., 2015. Atmospheric processing outside clouds increases soluble iron in mineral dust. Environ. Sci. Technol. 49 (3), 1472–1477. https://doi.org/10.1021/es504623x.
Sholkovitz, E.R., Sedwick, P.N., Church, T.M., Baker, A.R., Powell, C.F., 2012. Fractional solubility of aerosol iron: synthesis of a global-scale data set. Geochim. Cosmochim. Acta 89, 173–189. https://doi.org/10.1016/j.gca.2012.04.022.
Siefert, R.L., Johansen, A.M., Hoffmann, M.R., 1999. Chemical characterization of ambient aerosol collected during the southwest monsoon and intermonsoon seasons over the Arabian Sea: labile-Fe (II) and other trace metals. J. Geophys. Res. Atmos. 104 (D3), 3511–3526.
Spolaor, A., Vallelonga, P., Cozzi, G., Gabrieli, J., Varin, C., Kehrwald, N., Zennaro, P., Boutron, C., Barbante, C., 2013. Iron speciation in aerosol dust influences iron bioavailability over glacial-interglacial timescales. Geophys. Res. Lett. 40 (8), 1618–1623. https://doi.org/10.1002/grl.50296.
Tagliabue, A., Bowie, A.R., Boyd, P.W., Buck, K.N., Johnson, K.S., Saito, M.A., 2017. The integral role of iron in ocean biogeochemistry. Nature 543 (7643), 51–59. https://doi.org/10.1038/nature21058.
Takahashi, Y., Higashi, M., Furukawa, T., Mitsunobu, S., 2011. Change of iron species and iron solubility in Asian dust during the long-range transport from western China to Japan. Atmos. Chem. Phys. 11 (21), 11237–11252. https://doi.org/10.5194/acp-11-11237-2011.
Vincent, R.F., 2018. The effect of Arctic dust on the retrieval of satellite derived sea and ice surface temperatures. Sci. Rep. 8 (1), 9727. https://doi.org/10.1038/s41598-018-28024-6.
Wiederhold, J.G., Kraemer, S.M., Teutsch, N., Borer, P.M., Halliday, A.N., Kretzschmar, R., 2006. Iron isotope fractionation during proton-promoted, ligand-controlled, and reductive dissolution of goethite. Environ. Sci. Technol. 40 (12), 3787–3793. https://doi.org/10.1021/es052228y.
Wilke, M., Farges, F., Petit, P.E., Brown Jr., G.E., Martin, F., 2001. Oxidation state and coordination of Fe in minerals: an Fe K-XANES spectroscopic study. Am. Mineral. 86 (5–6), 714–730.
Xu, N., Gao, Y., 2008. Characterization of hematite dissolution affected by oxalate coating, kinetics and pH. Appl. Geochem. 23 (4), 783–793. https://doi.org/10.1016/j.apgeochem.2007.12.026.
Zhu, X., Prospero, J.M., Savoie, D.L., Millero, F.J., Zika, R.G., Saltzman, E.S., 1993. Photoreduction of iron(III) in marine mineral aerosol solutions. J. Geophys. Res. Atmos. 98 (D5), 9039–9046. https://doi.org/10.1029/93JD00202.
Zhuang, G., Yi, Z., Duce, R.A., Brown, P.R., 1992. Chemistry of iron in marine aerosols. Glob. Biogeochem. Cycles 6 (2), 161–173. https://doi.org/10.1029/92GB00756.